Jahangirnagar University
Journal of Geospatial Sciences
Volume 1, 2025; DOI: https://doi.org/10.59185/jgs.v1i1.269

Research Article

Projecting Climate Trends of Southwest Coastal Bangladesh under Global Climate Scenarios

Nasirul Haque [1, *], Salma Noor [2], Krishna Prosad Mondal [3], Shihab Ahmed Shahriar [2], Shahriar Md. Arifur Rahman [4], Rajsree Das Tuli [5]

[1] Assistant Leaf Officer, British American Tobacco Bangladesh, Jhenaidah-7300, Bangladesh
[2] PhD Candidate, Department of Earth and Atmospheric Sciences, University of Houston, USA
[3] IT Officer (Geospatial Analyst), Institute of Remote Sensing and GIS, Jahangirnagar University, Dhaka-1342, Bangladesh
[4] PhD Candidate, Environmental Sciences, University of Idaho, Idaho, USA
[5] PhD Candidate, Department of Geography and Environmental Sustainability, The University of Oklahoma, Norman, USA

**Corresponding Author: nasirulhaque00@gmail.com*

Abstract

Southwest coastal Bangladesh, situated within the Ganges-Brahmaputra-Meghna delta, is one of the world's most climate-vulnerable areas, confronting elevated sea levels, saline intrusion, tidal inundation, and cyclonic storms that threaten crops and livelihoods. Understanding long-term climatic patterns in this area is essential for developing localized adaptation and management solutions. This study aims to examine historical and projected patterns in temperature and precipitation to evaluate probable future climatic conditions under global climate scenarios. Future climate projections for the Khulna Division in the southwest part of Bangladesh using a statistical downscaling approach based on multiple Representative Concentration Pathways (2.5, 4.5, and 8.5) and Special Report on Emission Scenarios (SRES A2 and A1B). A Statistical Downscaling Model (SDSM) was used to downscale two Global Circulation Models (GCMs) viz CanESM2 and CGCM3. The models were evaluated against observed minimum and maximum temperature and precipitation data for the 30-year period 1987-2017. In addition, the downscaled climate variables were subjected to bias correction. During model calibration using NCEP predictors, the explained variances for CanESM2 and CGCM3 were 92.3% and 78% for Tmax, 28.02% and 45.36% for Tmin, and 9.28% and 10.11% for precipitation. The average R2 values during validation ranged from 0.82 to 0.89 for Tmax, 0.61 to 0.88 for Tmin, and 0.32 to 0.47 for precipitation. These results indicate good applicability of SDSM for downscaling daily minimum and maximum temperature and precipitation under different scenarios for future periods in the 2020s, 2050s, and 2080s. For CanESM2, changes in minimum annual temperature are projected to increase by 0.45°C, 0.46°C, and 0.63°C by 2080 for RCP 2.6, RCP 4.5 and RCP 8.5 scenarios, respectively. CGCM3 projected a maximum temperature increase of 0.32°C and 0.31°C by 2080 *under the SRES A2 and A1B scenarios, respectively. Precipitation is projected to increase 0.46mm, 0.71mm and 1.28mm for RCP 2.6, RCP 4.5 and RCP 8.5, respectively, by the end of this century and 0.77mm and 0.87mm under the A1B and A2 scenarios, respectively, for the same period.*

Keywords: Climate Model; Regional Scale; Downscaling; SDSM; GCM; RCP

1 Introduction

Local policymakers and development planners increasingly demand reliable climate information to address the growing threats posed by climate change and its projected consequences. The Intergovernmental Panel on Climate Change (IPCC, 2014; 2021) offers climatic estimates at global and continental scales for the conclusion of the twenty-first century, using accessible observational and modeled data. However, these projections are often inadequate to facilitate subnational adaptation efforts, which need regional or local forecasts for shorter timeframes-generally the next five to ten years. Policymakers furthermore pursue sector-specific analyses of the effects of climate change on agriculture, food security, public health, water resources, and demographic trends. Assessing vulnerabilities across various geographical scales facilitates a more accurate comprehension of climate change effects from global to local levels. Researchers have employed various methodologies and indices to provide location-specific climate information, each with distinct assumptions, benefits, and drawbacks. Downscaling approaches have been developed to refine coarse Global Climate Model (GCM) outputs into higher resolution estimates suitable for informed decision-making. However, downscaling poses methodological challenges, and no worldwide or national agency currently offers standardized recommendations to aid researchers and policymakers in selecting aims to support climate experts in understanding statistical downscaling techniques and interpreting their results to effectively communicate statistical downscaling techniques and interpreting their results for the successful transmission of localized climate forecasts.

The continued concentration of greenhouse gases in the atmosphere, primarily from fossil fuels flaming and land-use changes, has intensified global warming and disrupted the earth's energy balance (Wentz et al. 2007; Chu et al. 2010; Huang et al. 2011; Tuli et al. 2025). According to the IPCC's fifth assessment report (AR5) and subsequent updates, the global mean temperature (GMT) increased by approximately 0.85°C between 1880 and 2012 and is projected to increase by around 0.3°C to 4.8°C by the end of the twenty-first century depending on Representative Concentration Pathways (RCPs). Recent observations confirm an upward trend of about 0.13 °C per decade, with accelerated warming over the past two decades (IPCC, 2021). Rising global temperatures intensify the hydrological cycle, influencing water availability, food production, public health, energy demand, and ecosystem stability (Chu 2010; Jang et al. 2011; Tuli et al. 2025).

Global Climate Models (GCMs), commonly known as General Circulation Model (GCM), remain the primary tools for simulating and projecting climate variability and long-term change. These sophisticated, physics-based numerical models represent interactions among the atmosphere, oceans, land surface, and cryosphere (Wells et al., 2019). While important for understanding large-scale processes, GCMs typically operate at spatial resolutions of 250–600 km, which is insufficient for examining regional or local climate impacts (Straw et al., 2000; Willoughby et al., 2000). Bridging this gap requires downscaling techniques, which translate coarse GCM outputs into higher-resolution projections at regional or local scales (Wetterhall et al. 2006). Early applications of downscaling were concentrated in Europe and North America (Salzmann et al., 2007), but these methods are now widely used across Asia, including Bangladesh, to assess fine-scale climate impacts (Sharma, 2007; Akhtar, 2008; Elshamy et al., 2009; Huang et al., 2011).

Two principal approaches are used for downscaling GCM outputs: dynamical and statistical. The dynamical approach employs high-resolution Regional Climate Models (RCMs) nested within GCMs, typically at 5–50 km resolution (Chu et al. 2010). RCMs simulate local processes such as orographic effects, monsoonal dynamics, and extreme events. However, they are computationally intensive and sensitive to boundary conditions, requiring significant coordination between global and regional modeling centers (Fowler et al., 2007). In contrast, statistical downscaling, the method used in this study, establishes empirical relationships between large-scale atmospheric predictors and local climatic variables, enabling efficient generation of high-resolution projections with relatively modest computational resources (Willoughby and Wigley 1997; Straw and Clark 2003; Fowler et al. 2007).

Bangladesh's climate, like that of much of the world, has become increasingly erratic in recent years (Rahman 2013). Bangladesh, a densely populated and agriculturally dependent nation, faces numerous climate change-related threats, including floods, droughts, cyclones, tidal surges, sea-level rise, saltwater intrusion,soil salinity and waterlogging (Nasreen et al., 2023; World Bank, 2022; Haque et al., 2024). Consequently, incorporating climate change scenarios into development planning and sectoral policy formulation is crucial for maintaining agricultural production, ensuring food security, and promoting general socioeconomic stability (Rahman, 2013; World Bank, 2022).

Prior research has predominantly utilized coarse-resolution Global Climate Models (GCMs), which frequently fail to adequately represent the intricate variability of temperature and precipitation in coastal Bangladesh (Haque et al., 2021; Ahmed & Alam, 2020). To address this restriction, statistical downscaling strategies, such as the Statistical Downscaling Model (SDSM), have been used to provide localized predictions by using observed meteorological data and large-scale predictors (Wilby & Dawson, 2013; Mahmood et al., 2023). Nonetheless, these methodologies are constrained in southwest Bangladesh, namely in the Khulna Division, according to both the Special Report on Emission Scenarios (SRES) and the Representative Concentration Pathways (RCPs). This gap limits comprehension of how temperature and precipitation may change at a subnational level.

This study examines historical and projected climate changes in the Khulna Division using downscaled outputs from two General Circulation Models (CanESM2 and CGCM3) under the SRES (A2, A1B) and RCP (2.6, 4.5, 8.5) scenarios. This analysis assesses long-term trends

(1987–2017), evaluates the efficacy of the model, and forecasts future changes for the 2020s, 2050s, and 2080s to inform climate-resilient agriculture, water management, and policy formulation in this vulnerable coastal area.

2 Materials and Methods

The methodology section is divided into two parts: (i) a brief description of the study areas and the data, and (ii) quantitative techniques to project climate variability trends.

2.1 Study Area and Data Description

Khulna Division, located in the extreme southwest of Bangladesh, is one of the country's eight administrative divisions. It spans roughly 22,283 km², about one-sixth of the national land area (Fig 1) and extends from 21°34′ to 24°13′ N and 88°33′ to 89°58′ E. The division is bounded by the Ganges River to the north, the Garai-Madhumati-Baleswar-Haringhata river system to the east, the Bay of Bengal to the south, and the international border with India to the west.

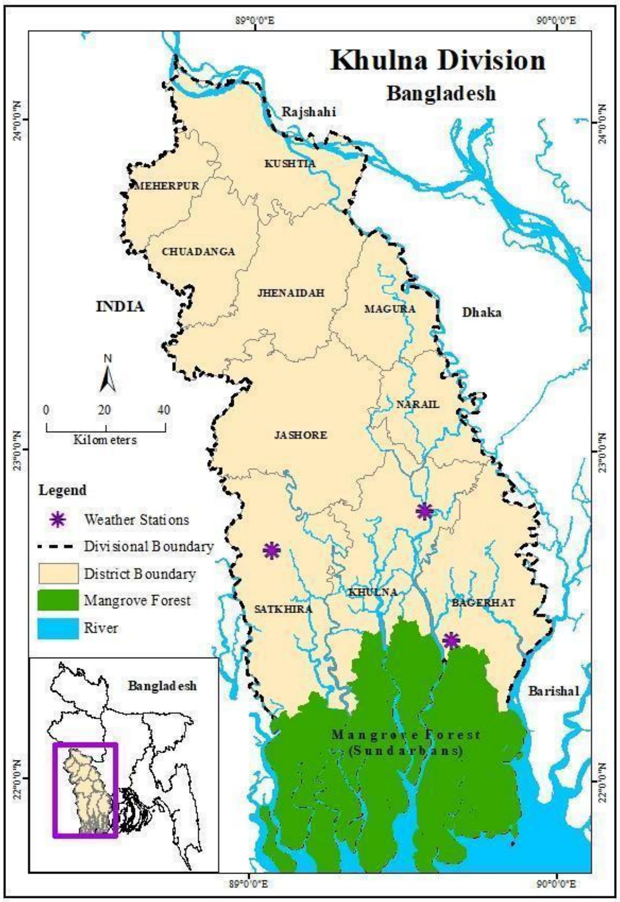

Figure 1: The southwestern administrative unit of Bangladesh

It occupies about 22,283 km2 (BBS, 1993) and had a population of 15,563,000 at the 2011 Census. Climate data (Minimum Temperature, Maximum Temperature and Precipitation) of the three weather stations in the Khulna division (Khulna, Mongla, Satkhira) are collected by the Bangladesh Meteorological Department (BMD). The data in this study comprises 31 years (1987-2017) of observation. The percentage of missing data is about 4%. The data cover more than thirty years because the study was based on the downscaling climate change projection for two variables (temperature and precipitation).

2.2 Brief description of the study areas and the data

The overall method has three parts: selecting GCMs to project climate scenarios, establishing a statistical relationship between GCMs and observed data to evaluate the Statistical Downscaling Model (SDSM), and downscaling the GCM output on the established statistical relationship.

Predictor selection is the first stage of the downscaling workflow. Candidate large-scale variables are screened against the local predictand, prioritizing those that yield higher explained variance and strong, physically interpretable correlations. Using the chosen predictors, the model is then calibrated against observations from the baseline period (1981-2010), after which the calibrated relationships are applied to GCM outputs to produce future simulations. Then, model validation is evaluated with bias correction by the statistical analysis followed by weather generation. The calibration period of the model is selected as 17 years, while the validation of the model is conducted for 10 years.

These generated scenarios are then used for time series analysis. The Mann-Kendal (M.K.) test is done to evaluate the trend of the scenarios. To interpolate the areas surrounded by the weather stations, spatial analysis is done by the IDW method.

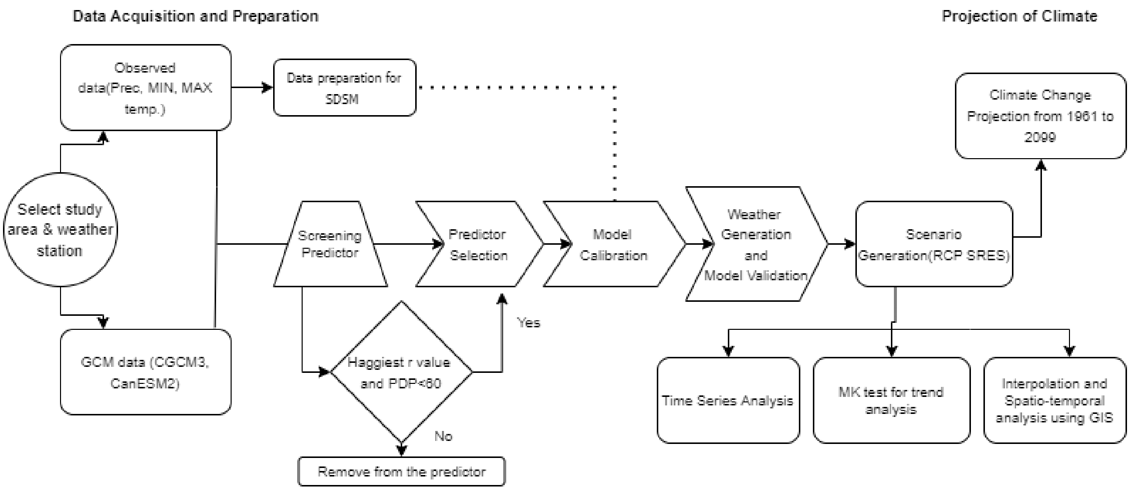

Figure 2: Methodology flow chart

2.3 General Circulation Model (GCM) Selection

A recommended practice is to analyze projections from more than one global climate model to capture inter-model (structural) uncertainty. Accordingly, this study employs two models: the second-generation Canadian Earth System Model (CanESM2) and the third-generation Coupled Global Climate Model (CGCM3).

2.4 Canadian Earth System Model (CanESM)

The second-generation Canadian Earth System Model (CanESM2), developed by the Canadian Centre for Climate Modelling and Analysis (CCCma), represents CCCma's fourth major coupled modeling effort and contributed to the IPCC Fifth Assessment Report (AR5). It is employed here primarily because it provides daily large-scale predictor fields that can be ingested directly by SDSM. For future projections, we use CanESM2 under multiple Representative Concentration Pathway (RCP) scenarios: RCP2.6, RCP4.5, and RCP8.5.

To establish empirical links with local observations during calibration, we also use large-scale atmospheric variables from the NCEP/NCAR Reanalysis-1. CCCma distributes a harmonized set of predictors for both CanESM2 and NCEP/NCAR that span the 1961-2005 period and include an identical suite of 26 variables (Table 1), ensuring consistency between reanalysis-based calibration and GCM-driven simulation. All predictor datasets were obtained from the Canadian Climate Data and Scenarios portal. The predictor grids have an approximately uniform horizontal resolution of ~2.8° × 2.8° in longitude and latitude (Wilby & Dawson, 2007).

Table 1: List of Predictor Variables (CanESM2)

Sl	Predictor	Description of predictor	Sl	Predictor	Description of predictor
1	mslpgl	Mean sea level pressure	**14**	p5zhgl	500hPa Divergence of true wind
2	p1_fgl	1000hPa Wind speed	**15**	p850gl	850hPa Geopotential
3	p1_ugl	1000hPa Zonal wind component	**16**	p8_fgl	850hPa Wind speed
4	p1_vgl	1000hPa Meridional wind component	**17**	p8_ugl	850hPa Zonal wind component
5	p1_zgl	1000hPa Relative vorticity of wind	**18**	p8_vgl	850hPa Meridional wind component
6	p1thgl	1000hPaWind direction	**19**	p8_zgl	850hPa Relative vorticity of wind
7	p1zhgl	1000hPa Divergence of true wind	**20**	p8thgl	850hPa Wind direction
8	p500gl	500hPa Geopotential	**21**	p8zhgl	850hPa Divergence of true wind
9	p5_fgl	500hPa Wind speed	**22**	Prcpgl	Total precipitation
10	p5_ugl	500hPa Zonal wind component	**23**	s500gl	500hPa Specific humidity
11	p5_vgl	500hPa Meridional wind component	**24**	s850gl	850hPa Specific humidity
12	p5_zgl	500hPa Relative vorticity of wind	**25**	Shumgl	1000hPa Specific humidity
13	p5thgl	500hPa Wind direction	**26**	Tempgl	Air temperature at 2m

Source: Climate Change Cell

2.5 Coupled Global Circulation Model (CGCM)

The CGCM3 is CCCma's third-generation coupled climate model. It retains the ocean component from CGCM2 but incorporates a substantially upgraded atmospheric core, AGCM3 (Atmospheric Canadian GCM, version 3), which introduces several key improvements: the Canadian Land Surface Scheme (CLASS) for land-atmosphere exchanges, revised treatment of water-vapor transport, and updated cumulus parameterization. Collectively, these changes enhance the model's representation of surface energy and moisture fluxes as well as convective processes.

For large-scale predictors, upper-air fields were archived at 6-hourly intervals on a spectral T47 grid with 31 vertical (η) levels (model top ~ 50 km). Surface and near-surface variables are provided at daily resolution on a global Gaussian grid of 96 longitudes × 48 latitudes (~ 3.75° × 3.75°). The full list of CGCM3 predictor variables used in this study appears in Table 2.

Table 2: List of Predictor Variables (CGCM3)

Sl	Predictors	Description of predictors	Sl	Predictors	Description of predictors
1	mslp	Mean sea level pressure (Pa)	13	X5	500 hPa wind direction (°)
2	S10	1,000 hPa Wind speed (m/s)	14	D5	500 hPa divergence (s^{-1})
3	U10	1,000 hPa U component (m/s)	15	S8	850 hPa wind speed (m/s)
4	V10	1,000 hPa V component (m/s)	16	U8	850 hPa U component (m/s)
5	C10	1,000 hPa vorticity (s^{-1})	17	V8	850 hPa V component (m/s)
6	X10	1,000 hPa wind direction (°)	18	C8	850 hPa vorticity (s^{-1})
7	D10	1,000 hPa divergence (s^{-1})	19	Z8	850 hPa geopotential height (m^2/s^2)
8	S5	500 hPa wind speed (m/s)	20	X8	850 hPa wind direction (°)
9	U5	500 hPa U component (m/s)	21	D8	850 hPa divergence (s^{-1})
10	V5	500 hPa V component (m/s)	22	H5	500 hPa specific humidity (kg/kg)
11	C5	500 hPa vorticity (s^{-1})	23	H8	850 hpa specific humidity (kg/kg)
12	Z5	500 hPa geopotential height (m^2/s^2)	24	H_{10}	1,000 hPa specific humidity (kg/kg)

Source: Climate Change Cell

2.6 Statistical Downscaling Model (SDSM)

The Statistical DownScaling Model (SDSM) combines a transfer-function (multiple-regression) component with a stochastic weather generator, linking large-scale atmospheric drivers to local daily weather. In practice, circulation and moisture fields at synoptic scales are used to condition the parameters of the weather generator through linear regression, yielding site-specific simulations suitable for impacts assessment. Compared with simple weather generators or weather-typing schemes, SDSM is designed to represent interannual variability more accurately.

SDSM requires two daily data streams: (i) local predictands (e.g., station-scale maximum/minimum temperature, precipitation), and (ii) large-scale predictors drawn from reanalysis (e.g., NCEP) and from the nearest GCM grid cell over the study area. Predictor selection is undertaken within SDSM using correlation and partial-correlation diagnostics to identify a parsimonious, physically interpretable set of predictors prior to calibration and scenario generation.

Statistical downscaling requires developing quantitative relationships between large-scale atmospheric variables/GCM outputs (predictors) and local-scale observed variables (predictands) (Wilby et al., 2004). Mathematically, this relationship can be written as (Dibike and Coulibaly, 2005):

$$Y = f(X)$$

where,
Y = Predictand,
X = Predictor, and
f = Transfer function, which has to be determined empirically from historical observations.

2.7 Model Setup

Before estimating predictor-predictand relationships, we configured key SDSM options to ensure consistency across datasets and to maximize agreement between simulated and observed statistics, following the SDSM v4.2 guidance. A critical step is aligning calendar conventions with the source data. For station observations and NCEP reanalysis used in calibration, we adopted the Gregorian calendar (including leap years). For GCM-driven scenario runs (CanESM2 and CGCM3), we used a 365-day, no-leap setting, reflecting the way these model outputs are archived. The analysis window for the present study was defined as 01-01-1981 to 31-12-2010, matching the 31-year baseline used throughout the evaluation and downscaling workflow.

Model configuration followed standard SDSM conventions. Temperatures (Tmin, Tmax) were permitted to take negative values, whereas precipitation was constrained to be non-negative. The event threshold was set to 0 for temperature variables and 0.1 mm day^{-1} for precipitation, so days with $\leq$0.1 mm were treated as dry. All input series used -999 as the missing-data sentinel; SDSM automatically excludes these entries during calibration and when computing summary statistics. For the stochastic weather generator, the pseudorandom seed was left unfixed, allowing each run of the generator (and scenario module) to produce a distinct ensemble realization.

2.8 Quality control and data transformation

The quality control function assists in checking for errors in the input data by giving general information such as mean value, maximum and minimum value, number of missing data, total number of values, and so on. The data transformation operation provides the facility of transforming either the predictor variable or the predictand by selecting the desired form of transformation such as logarithm, power, inverse, lag, or binomial. However, no modification was done for this study.

2.9 Predictor screening and selection

Choosing appropriate large-scale predictors is the most consequential step in a statistical downscaling workflow because it shapes the behavior of the resulting local projections. We used SDSM's Screen Variables utility to guide selection, examining monthly, seasonal, and annual relationships between each candidate predictor and the station-scale predictand. The screening combined (i) explained variance and simple correlation, (ii) partial correlation to assess each predictor's unique contribution in the presence of others, and (iii) visual scatterplots to check linearity and outliers. Predictors that exhibited strong mutual correlation were considered redundant and removed to avoid collinearity; the final set favored parsimony and physical interpretability.

Initial screening drew on the NCEP/NCAR Reanalysis-1 predictor archive covering 1961–2005, ensuring consistency with the GCM predictor suite distributed for SDSM. Because daily precipitation typically shows weaker linear association with large-scale fields than Tmax or Tmin, selection was conducted month by month, allowing the retained predictors to vary seasonally. After screening, the retained predictors were used to estimate the transfer-function coefficients and saved as monthly .PAR files, which subsequently drove stochastic weather generation and scenario simulations.

From the 26 NCEP predictors made available with the CanESM2/NCEP bundle, five variables with high explained variance were shortlisted: ncepp500, ncepp5zas, ncep_thas, nceptempas, and ncepshumas. Partial-correlation analysis indicated that ncepp (pressure) was strongly collinear with other candidates and thus contributed little unique information; it was therefore excluded. The remaining four predictors showed consistent associations with the target variables in the scatterplots and were retained as the final set. The same screening protocol was applied to each predictand (Tmax, Tmin, precipitation) and station, yielding predictor sets tailored to variable and season.

Table 3: Correlation Matrix Obtained from SDSM for Mongla Station Using CanESM2

Sl.	Code	Predictor	R1 (%)	Pr(%)	P	PDP(%)
17	**p8_v**	**850 hpa meridional velocity**	**4.2**			
2	p1_f	Surface air flow strength	2.9	2.4	0.18	79
4	p1_v	Surface meridional velocity	2.8	0.6	0.55	17
5	**p_z**	**Surface vorticity**	**4.0**	**2.3**	**0.00**	**85**
6	p1_th	Surface wind direction	3.0	0.6	0.17	13
7	p_zh	Surface divergence	4.3	3.4	0.00	41
13	**p5_th**	**500 hpa wind direction**	**3.2**	**2.5**	**0.29**	**6.25**
15	p8_f	850 hpa airflow strength	3.4	3.4	0.00	70
1	**mslp**	**Mean sea level pressure**	**2.9**	**1.0**	**0.00**	**9.25**
18	p8_z	850 hpa vorticity	2.6	3.8	0.00	69
22	Prcp	Surface precipitation	2.6	1.6	0.00	42.0
26	Temp	Surface mean temperature	3.4	1.8	0.00	47

2.10 Model Calibration

Following the screening step, we estimated transfer functions linking the selected large-scale predictors to each station-scale predictand and saved the resulting coefficients as monthly parameter (.PAR) files. SDSM provides two optimization choices. Dual simplex and ordinary least squares (OLS) and we adopted OLS for all variables and stations. Calibration was performed at a monthly resolution, yielding twelve regression equations per variable (one for each calendar month).

Model specification followed standard SDSM practice: unconditional formulations were used for Tmin and Tmax, assuming a direct predictor-predictand relationship, whereas precipitation was modeled conditionally, acknowledging the intermediate occurrence/intensity process characteristic of wet-day generation. Statistical significance was assessed at $\alpha = 0.05$. As the distribution of daily precipitation is normally skewed, the model was transformed to the fourth root for precipitation to convert it into a normal distribution. No transformation was applied for daily maximum and minimum temperature considering the normal distribution.

The available 30 years of observed historical data (i.e., 1987-2017) were divided into two groups. The first 26 years (1987-2013) were used for calibration and the remaining 4 years (2013-2017) were kept for validation processes.

The observational record spanning 1987-2017 was partitioned into an in-sample calibration period (1987–2013) and an out-of-sample validation period (2014-2017). Variance inflation and bias correction were also adjusted during calibration. Variance inflation helps to control the magnitude of variance in downscaled daily weather variables, and bias correction compensates for the tendency of over and under estimation of the mean of conditional processes by the downscaling model (Wilby and Dawson 2007). The default value of 12 for variance inflation produces approximately normal variance inflation, and the default value of 1 in bias correction indicates no bias correction (Wilby and Dawson 2013). For temperature, SDSM default settings were retained. For precipitation, parameters were iteratively tuned by adjusting occurrence/intensity and variance-inflation options; until the simulated monthly means, variance, and wet-day frequency closely matched observations. A similar procedure was followed for calibrating all the variables for all the stations.

2.10.2 Validation of SDSM results

The time series of station data and NCEP reanalysis data were partitioned into an in-sample calibration period (1987-2013) and an out-of-sample validation period (2013-2017). Model performance for temperature (Tmax, Tmin) was assessed using monthly means and variance, while precipitation performance was evaluated using mean wet-spell length and mean dry-spell length.

SDSM's summary-statistics module was used to compute these diagnostics along with auxiliary measures (e.g., dispersion and autocorrelation) for both observed and simulated series. The Compare Results utility then provided side-by-side visualizations to facilitate rapid appraisal of model fidelity. Where systematic discrepancies were evident, we iteratively adjusted variance-inflation and applied monthly bias corrections until the simulated climatology aligned with observations specifically, matching monthly means for Tmax/Tmin and wet/dry-spell characteristics for precipitation at each station.

2.10.3 Bias correction

The bias correction approach is used to eliminate the biases from the daily time series of downscaled data (Salzmann et al. 2007). To reduce residual systematic error we applied a simple month-wise bias adjustment following common practice. Additive corrections were used for temperature and multiplicative factors for precipitation, computed from a control period (e.g., 2003-2013) by comparing downscaled "historical" simulations with observations.

$T_{deb} = T_{scen} - (T_{sim} - T_{obs})$ ………………………………………………………….. (i)

$P_{deb} = P_{scen} \times (P_{obs}/P_{sim})$ …………………………………………………………… (ii)

Where,

T = Temperature and P= Precipitation

T_{deb}/P_{deb} = bias corrected temperature and precipitation

T_{scen}/P_{scen} = Scenario data downscaled by SDSM

T_{obs} = Observed temperature and precipitation

2.10.4 Scenario generation

The Scenario Generator operates analogously to the weather generator but is driven by GCM predictors rather than reanalysis. After validating the calibrated models, we applied the same monthly parameter (.PAR) files derived from the screening and calibration steps to downscale future conditions using outputs from CanESM2 (RCP2.6/4.5/8.5) and CGCM3 (A2/A1B).

According to Nigatu (2013), an average of 20 individual ensemble outputs perform well. A large number of ensembles do not produce improved results. Hence, to characterize uncertainty while maintaining computational efficiency, we produced 20 ensemble realizations per station-variable-scenario. Prior evaluations have shown that increasing the ensemble size beyond this threshold offers diminishing returns and can inflate inter-member spread without improving central estimates. The procedure was repeated for all scenarios and all stations, yielding daily downscaled time series that were subsequently aggregated into standard climatological windows for analysis.

2.10.5 Statistical Evaluation of the Model

Among the variety of model evaluation techniques available (Moriasi et al. 2007), the performance of the SDSM in this study was evaluated based on quantitative statistics: correlation coefficient, coefficient of determination (R2), root mean square error (RMSE), the Durbin-Watson (D.W.) test, and time series analysis with the Mann-Kendall (M.K.) test. Then uncertainty analysis was conducted to have confidence in the climate scenarios downscaled from GCM outputs. In this study, uncertainty analysis was regulated by hypothesis testing.

3.8.6 Correlation Coefficient

The correlation coefficient (r) is the measure of the degree of a linear relationship between observed and simulated data. It ranges from -1 to 1. The higher or lower the value of r from 0, the more positive or negative the relationship, respectively; 0 represents no linear relationship. It is represented mathematically as:

$$r = \frac{\sum_{i=1}^{n} (x_i - x_{mean}).(y_i - y_{mean})}{\sqrt{\sum_{i=1}^{n} (x_i - x_{mean})^2 . \sum_{i=1}^{n} (y_i - y_{mean})^2}} \quad \text{(iv)}$$

Where,

x_i = i^{th} observed value, (i= 1, 2, 3,……, n)

x_{mean} = mean of observed value,

y_i = i^{th} simulated value,

y_{mean} = mean of simulated value

2.10.7 Coefficient of determination

The coefficient of determination (R^2) compares the explained variance of modeled data with the total variance of the observed data (Liu et al. 2011) with a value ranging from 0 to 1. A higher value of R^2 represents better model performance. The mathematical representation is:

$$R^2 = \frac{\sum_{i=1}^{n} (y_i - y_{mean})^2}{\sum_{i=1}^{n} (x_i - x_{mean})^2} \quad \text{(v)}$$

Where,

x_i = i^{th} observed value, (i= 1, 2, 3,……, n)

x_{mean} = mean of observed value,

y_i = i^{th} simulated value,

y_{mean} = mean of simulated value

2.10.9 Root Mean Squared Error (RMSE)

The RMSE is an error index used to measure the difference between observed and simulated values. The RMSE value of 0 represents a perfect fit (Moriasi et al. 2007).

$$RMSE = \sqrt{\frac{\sum_{i=1}^{n} \quad (x_i - y_i)^2}{n}} \qquad \text{(vi)}$$

Where,

x_i = i^{th} observed value, (i= 1, 2, 3,……, n)

y_i = i^{th} simulated value

n = Number of observations

2.11 Mann-Kendall (M.K.) test

The non-parametric Mann-Kendall test is commonly employed to detect monotonic trends in series of environmental data, climate data or hydrological data. The null hypothesis, H0, is that the data come from a population with independent realizations and are identically distributed. The alternative hypothesis, Ha, is that the data follow a monotonic trend (Pohlert, 2018).

A p-value < 0.05 indicates that there is (monotonic) trend and if tau is +ve, an increasing trend, and if tau value is -ve, a decreasing trend p-value > 0.05, no monotonic trend, away from the monotonic trend. In our study, the Mann-Kendall test was used to represent the presence of a trend.

3 Results

The selected NCEP predictors for CanESM2 and CGCM3 are shown in Figure 3. “Temperature at 2m height” was the super predictor for T_{max} and T_{min} for every model. As for precipitation, *ncepmslp* and *ncepshum, ncepp5_th and p8_v* (specific humidity) were selected as predictors for Khulna, while *ncepp1_v*, *ncepp500*, *ncepp8_u*, and *ncepp8_th* were selected as predictors for Mongla and Satkhira for both models. For Khulna, Mongla, and Satkhira, *ncepp5_z*, *ncepp8_v*, and *ncepp8_th* showed the best correlation with the observed data, respectively. Therefore, these predictors are super predictors for precipitation. They showed a significant relation with the predictand for CanESM2 and CGCM3 during calibration. The selection of the predictors was quite similar to that in the studies by Chu et al. (2010), Huang et al. (2011), Mahmood and Babel (2013), and Binti Pg et al. (2018). Figure 3 represents the total selector predictors for the Khulna division.

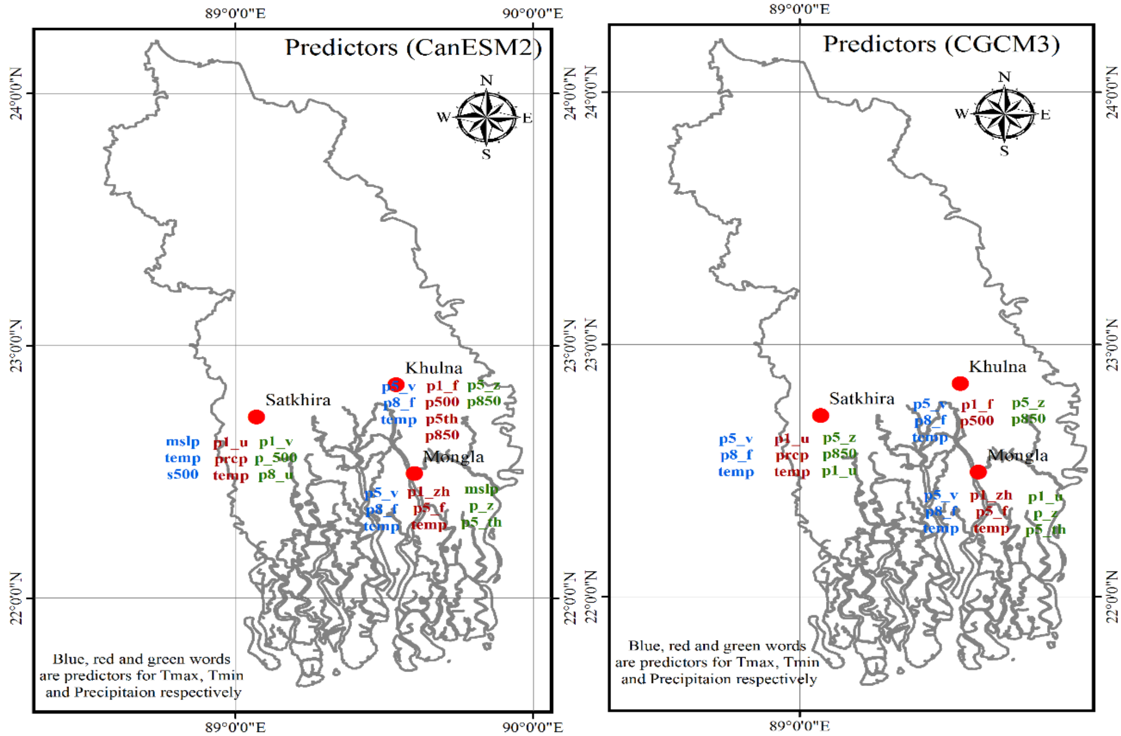

Figure 3: Predictors selected for the climate model

3.1 Calibration

This study used a monthly sub-model for the calibration process. Table 4.1 presents the calibration results for the models. The results were expressed in mean explained variance (E.V.) and standard error of the mean (S.E.). The explained variances for temperature were much higher than for precipitation. As confirmed by Wilby et al. (2002), this variation occurred due to the heterogeneous behavior of precipitation. The percentage of E.V. for temperature is most likely greater than 70%, while precipitation is not more than 40% (Wilby et al. 2002). The results of the calibration of this study also showed similar performance. The explained variances of T_{min} for CanESM2 and CGCM3 were 80.1% and 80.2%, respectively. The S.E. and MAD values of calibrated temperature were much closer to the predictand. However, precipitation showed the same performance for CanESM2 (10.2%) and CGCM3 (10.2%). There was a good deviation in S.E. and MAD between predictors and predictands for its conditional characteristic. The results shown in Table 4.1 are comparable to some previous studies such as Wilby et al. (2002), Gagon et al. (2005), Dibike et al. (2007), Liu et al. (2008), Bing and Jiahu (2010), Huang et al. (2011), Nguyen (2002), Souvignet and Heinrich (2011), Nigatu (2013), and Hasan et al. (2017). In this study, the range of mean explained variance for minimum temperature was 73.2-82.8% for CanESM2 and 74.2-83.0% for CGCM3. The results of the calibration with the mean percentage of E.V. and mean S.E. for two models at each station are also given in Table 4.1. For T_{max}, the highest (92.35%) and lowest (77.27%) explained variances were found at Khulna and Satkhira, respectively, for CanESM2. In comparison, the percentage of E.V. was always above 77% for all stations. The CGCM3 model showed similar results to CanESM2. For temperature, the model showed the best and worst performances for Khulna (92.35%) and Satkhira (77.27%), respectively. For T_{min}, the highest (87.32%) and lowest (26.47%) E.V. were found at Mongla and Satkhira, respectively, for CanESM2. The percentage of E.V. was always above 26% for all stations. Unlike CanESM2, CGCM3 showed E.V. above 45% for all stations. For precipitation, the best and worst performances were seen at Satkhira (9.52%) and Mongla (7.93%), respectively. However, for precipitation, the models showed an exception from temperature. Khulna had the highest (9.28% for CanESM2 and 9.52% for CGCM3) E.V. among all other stations, whereas Mongla had the lowest (7.93% for CanESM2 and 8.68% for CGCM3). According to Wilby et al. (2002), precipitation is a heterogeneous climate variable and is difficult to simulate accurately. Furthermore, the percentage of E.V. of temperature is most likely greater than 70%, while precipitation is most likely lower than 40%. The calibration followed the instructions and performed well according to Wilby et al. (2002). The calibration of the climate data had been processed for 30 years (1981-2010). According to the calibration results, GCMs developed the scenarios for temperature and precipitation.

Table 4: Result of Calibration Procedure Period (Individual Stations)

Weather Stations	**Model**	**T_{max}**		**T_{min}**		**Precipitation**	
		EV (%)	SE (°C)	EV (%)	SE (°C)	EV (%)	SE (°C)
Khulna	CanESM2	92.35	0.0523	28.02	0.0436	9.28	0.1207
	CGCM3	78.11	0.0436	45.36	0.0411	10.11	0.1302
Satkhira	CanESM2	77.27	0.0437	26.47	0.0419	8.73	0.1568
	CGCM3	80.45	0.0416	51.23	0.044	9.52	0.1537
Mongla	CanESM2	86.20	0.0416	87.32	0.0445	7.93	0.1386
	CGCM3	78.09	0.0362	54.32	0.032	8.68	0.1396

3.2 Validation of SDSM without bias correction

To validate the SDSM for T_{min} , T_{max}, and precipitation, five (three from CanESM2 and two from CGCM3) sets of data were generated from 2001 to 2010, forcing NCEP, RCP 2.6, RCP 4.5, RCP 8.5, A2, A1B, and B2 scenarios. The models were then validated without bias correction for two GCMs (Table-4.2). The datasets of CGCM3 were denoted as C3A2 and C3A1B. For T_{min}, T_{max} in CGCM3, the NCEP variables showed better validation results (R^2 = 0.81) than C3A2 and C3A1B. For CanESM2, the NECP and C2R8.5 showed the highest R^2

values and lowest RMSE values. On the other hand, the performance for simulating precipitation was not satisfactory in every case. As for the conditional process, the R^2 value was lower than that of the mean temperature for NCEP variables. Therefore, the behavior of SDSM was accepted, and it would be used for the projection of future climatic variables, i.e., T_{max}, T_{min}.

Table 5: Statistical comparison of observed and downscaled (without bias correction) daily temperature and precipitation by models during validation (2001–2010) *

Model	Scenario	T_{max}		T_{min}		Precipitation	
		R^2	RMSE	R^2	RMSE	R^2	RMSE
CGCM3	NCEP	0.81	1.34	0.68	0.34	0.11	09.05
	C3A2	0.79	1.98	0.57	0.27	0.20	11.25
	C3A1B	0.80	1.32	0.63	0.19	0.24	11.40
CanESM2	NCEP	0.85	1.21	0.67	0.28	0.17	11.20
	C2R2.6	0.81	1.32	0.59	0.42	0.27	09.87
	C2R4.5	0.78	1.27	0.64	0.36	0.22	10.52
	C2R8.5	0.85	1.05	0.69	0.31	0.31	8.530

3.3 Validation with Bias Correction

Unlike the validation results on temperature, this study did not find satisfactory results for precipitation. To get more reliable results, a simple bias correction technique (Salzmann 2007) was applied during the validation period. In terms of precipitation, the R^2 value increased after the bias correction for these models. The statistical techniques showed a promising result for mean temperature as explained above. The R^2 value was always above 0.82 for max temperature, 0.61 for min temperature and for the validation period after bias correction. The main outcome of this bias correction indicates lesser values of RMSE. This study's lower RMSE value and higher R^2 and NSE value clearly demonstrated the better efficiency of SDSM in simulating the daily temperature and precipitation data using bias correction.

Table 6: Statistical comparison of observed and downscaled (with bias correction) daily temperature and precipitation by models during valition (2001–2010)

Model	Scenario	T_{max}		T_{min}		Precipitation	
		R^2	RMSE	R^2	RMSE	R^2	RMSE
CGCM3	NCEP	0.87	1.01	0.61	0.34	0.32	8.15
	C3A2	0.82	0.87	0.78	0.27	0.46	7.25
	C3A1B	0.85	0.72	0.88	0.19	0.34	8.40

Model	Scenario	T_{max}		T_{min}		Precipitation	
		R^2	RMSE	R^2	RMSE	R^2	RMSE
CanESM2	NCEP	0.86	0.23	0.82	0.28	0.37	9.53
	C2R2.6	0.82	0.67	0.72	0.42	0.47	8.11
	C2R4.5	0.87	0.77	0.65	0.36	0.46	9.29
	C2R8.5	0.89	0.67	0.72	0.31	0.43	7.54

3.5 Downscaling future climate

The overall T_{max}, T_{min} and precipitation projections for every scenario are given in Table 6. The downscaled temperature showed an increasing trend in scenarios. In Khulna Division, the minimum and maximum annual temperature under the RCP 2.6 scenario may increase by 0.38°C and 0.23°C in the 2020s, 0.39°C and 0.38°C in the 2050s, and 0.45°C and 0.38°C by the 2080s, respectively, compared to the baseline period. Under the RCP 4.5, the stabilization scenario, the T_{min} and T_{max} might both increase by 0.46°C by the end of the century. RCP 8.5 showed the highest increase compared to the other two scenarios for all the time windows, with the maximum temperature increase reaching 0.99°C by the end of the century. On the other hand, , the annual minimum temperature may increase up to 0.60°C by the 2080s for the A2 scenario and 0.40°C for the A1B scenario.

Table 7: Future changes in annual min, max temperature (°C) and precipitation (mm) with respect to observed climate data under RCP2.6, RCP 4.5, RCP 8.5 and A2, A1B

Variable	Epoch	RCP 2.6	RCP 4.5	RCP 8.5	A2	A1B
T_{min}	2020s	0.38	0.38	0.38	0.33	0.21
	2050s	0.39	0.39	0.43	0.49	0.32
	2080s	0.45	0.46	0.63	0.60	0.40
T_{max}	2020s	0.23	0.31	0.53	0.24	0.21
	2050s	0.38	0.41	0.74	0.32	0.31
	2080s	0.38	0.46	0.99	0.50	0.35
Precipitation	2020s	0.41	0.59	0.42	0.57	0.33
	2050s	0.52	0.63	0.73	0.62	0.42
	2080s	0.47	0.71	1.28	0.87	0.77

The projection for precipitation (compared to the levels of 2010) is likely to exceed 0.41 mm by 2080 in all scenarios for Khulna regions and could reach as much as 1.28 mm (for RCP

8.5). Emission scenario A1B shows the lowest increment in precipitation compared to the other scenarios of RCP for all the time windows, reaching the level of 0.47 mm by the end of the century. Under the stabilization scenario RCP 4.5, precipitation may increase by 0.71 mm by the end of the century.

The table reveals that the projections of annual minimum, maximum temperature and precipitation significantly followed the storyline of the climate scenarios given by IPCC. The values of the future changes of temperature are quite different in magnitude or amount but identical in pattern to the storyline. All the scenarios showed incremental changes in values except for RCP 2.6.

To predict a value for any unmeasured location, the Kriging method was used to interpolate the measured values surrounding the prediction location. It was observed that the southwest part of the region was more vulnerable than the others. Specifically, Satkhira and Mongla showed a high temperature in every scenario (Figure 4). The interpolation results showed a positive trend of precipitation across all the divisions for every scenario, and the southwest part of the division had higher rainfall than the eastern region. Thus, spatial interpolation of the data for the division showed an increment of precipitation in the future which followed the storyline of the RCP and SRES scenarios provided by IPCC.

To validate the time series, the Mann-Kendall test (Table 8) was performed to get a comprehensive analysis of the trend of precipitation change in the Khulna Division. The results in Table 4.5 were obtained from the Mann- Kendall test for the temperature and precipitation data of the climate models. Every model showed a positive tau value and a lower *p*-value ($p > 0.05$). Rejecting the null hypothesis (H_0) indicated that there was a trend in the time series, while accepting H_0 indicates no trend was detected.

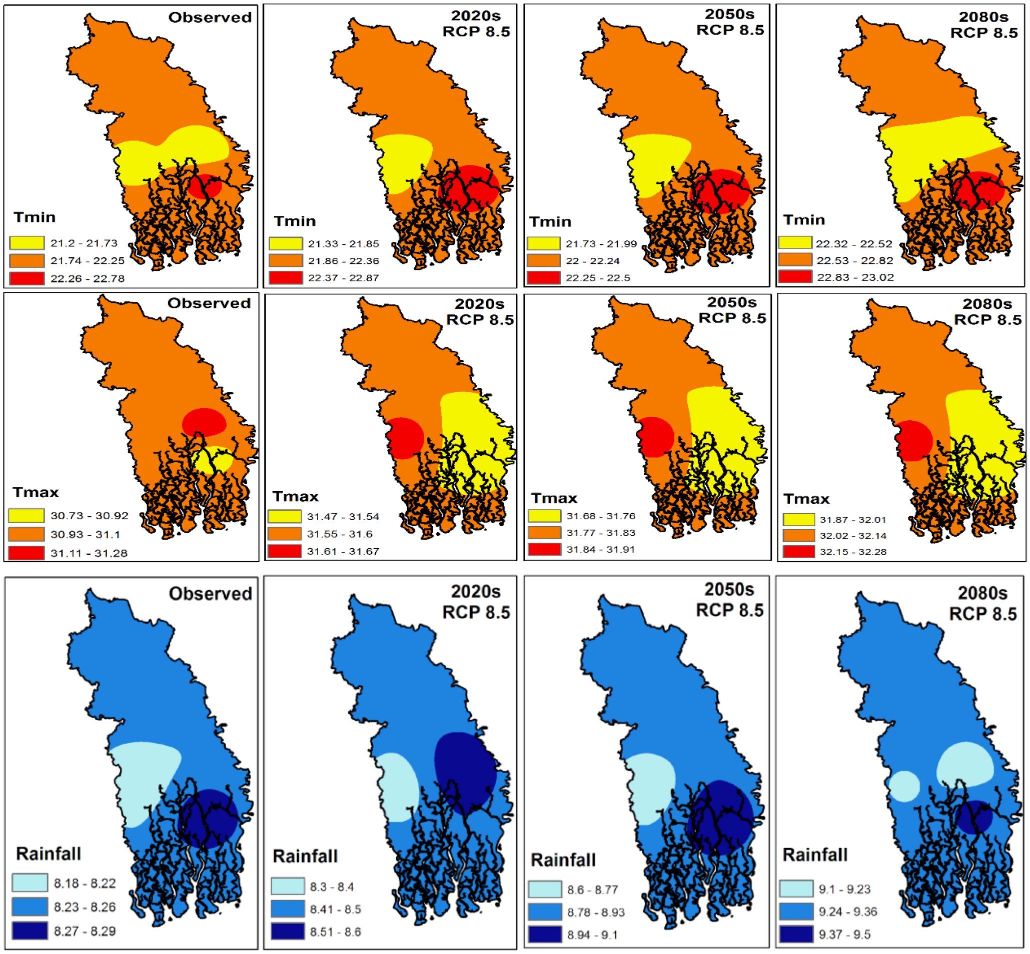

Figure 4: Changes in min, max temperature and precipitation in Khulna division under the RCP 8.5 scenario

Table 8: Summary statistics of time series analysis of the scenarios and observed data (precipitation)

Model	**Scenario**	**Mann-Kendall (M.K.) Test**				
		Tau Value	**M.K. score**	**Sen's Slope**	***p*-value (alpha = 0.05)**	**Test interpretation**
CanESM2	RCP 2.6	0.1259	520	0.0049	0.0005	Reject H_0
	RCP 4.5	0.2173	897	0.0127	0.0047	Reject H_0
	RCP 8.5	0.5703	2479	0.0325	< 0.0001	Reject H_0
CGCM3	A1B	0.5517	2423	0.0204	< 0.0001	Reject H_0
	A2	0.6818	2821	0.0266	< 0.0001	Reject H_0
Observed		0.0374	37	0.0047	0.0492	Reject H_0

Table 9: Summary statistics of time series analysis of the scenarios and observed data (T_{max})

Model	Scenario	Mann-Kendall (M.K.) Test				
		Tau Value	M.K. score	Sen's Slope	p-value (alpha=0.05)	Test interpretation
CanESM2	RCP 2.6	0.0124	574	0.0019	<0.0001	Reject H_0
	RCP 4.5	0.0247	759	0.0043	<0.0001	Reject H_0
	RCP 8.5	0.0458	867	0.0102	<0.0001	Reject H_0
CGCM3	A1B	0.0247	645	0.0053	<0.0001	Reject H_0
	A2	0.0557	695	0.0077	<0.0001	Reject H_0
Observed		0.1778	176	0.0049	0.0870	Reject H_0

Table 10: Summary statistics of time series analysis of the scenarios and observed data (T_{min})

Model	Scenario	Mann-Kendall (M.K.) Test				
		Tau Value	M.K. score	Sen's Slope	p-value (alpha=0.05)	Test interpretation
CanESM2	RCP 2.6	0.0127	527	0.0002	<0.0001	Reject H_0
	RCP 4.5	0.0211	762	0.0007	<0.0001	Reject H_0
	RCP 8.5	0.0457	1057	0.0112	<0.0001	Reject H_0
CGCM3	A1B	0.0347	645	0.0004	<0.0001	Reject H_0
	A2	0.0357	687	0.0008	<0.0001	Reject H_0
Observed		0.1778	176	0.0049	0.0870	Reject H_0

The results are statistically significant for rejecting the null hypothesis. The risk of rejecting the null hypothesis H_0 while true is lower than 0.01% - 0.05%. The test score simply demonstrates the strong trends which met the storyline instructions of IPCC. The RCP 8.5 and A2 scenarios had the highest emission scenario according to the M.K. score.

The M.K. test for observed temperature and precipitation over the course of the 31 years of collected data indicated that the trend is positive and that climate change has occurred. Figures 5 and 6 depict the overall future scenarios of minimum temperature, maximum temperature, and precipitation in the study area according to the models.

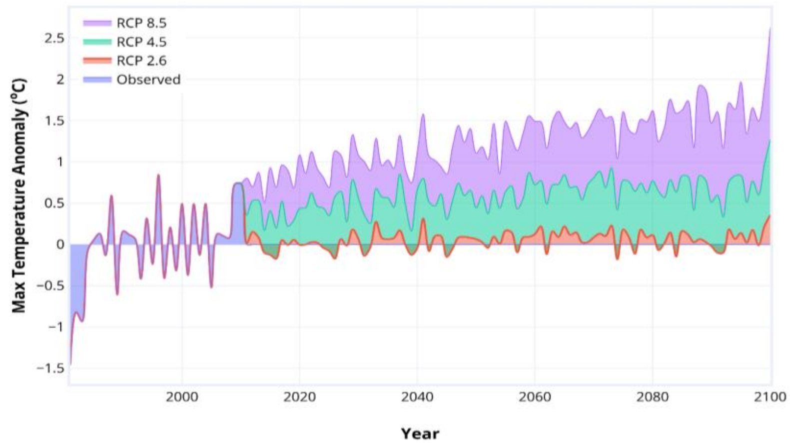

Figure 5: Climate scenarios of T_{max} and T_{min} in the Khulna division

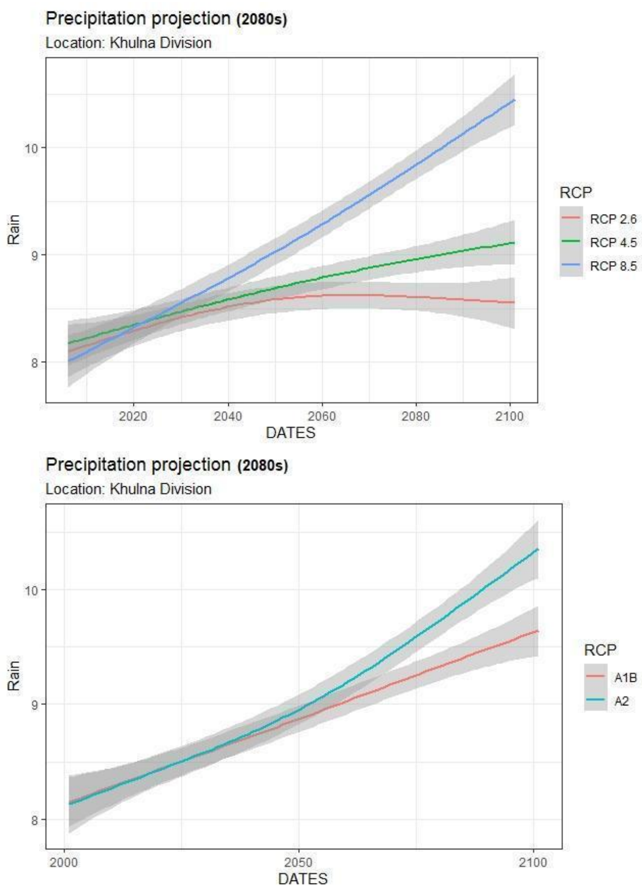

Figure 6: Climate scenarios of precipitation in the Khulna division (CanESM, cGCM)

Precipitation is considered a driver of the hydrological cycle, and thus any change in precipitation will change all the components of this cycle, including runoff, evapotranspiration, and stream flow. The change in precipitation across Khulna Division is spatially uniform, and a significant pattern of change has been confirmed as some researchers found an increasing trend and others saw a decreasing trend. The variations in precipitation over time and space may be due to the inherent characteristics of the CMIP5 model (i.e., CanESM2) used in this study. Liu et al. (2014) studied seasonal and regional biases in CMIP5 precipitation simulations and provided detailed insights on how CMIP5 models work in simulating summer and winter precipitation at different geographical locations and climatic conditions.

The results of this study reveal that most of the CMIP5 models underestimate summer precipitation and overestimate winter precipitation. Hence, it is better to use multiple models to enhance the accuracy and plausibility of the results. The two most important contributions of this study are time series analysis using the Mann-Kendall (M.K.) test and spatial analysis (interpolation by Kriging method). The M.K. test of time series analysis statistically proved the climate change projections which was then confirmed as visualization by Interpolation of the values.

4 Discussion

The Statistical Downscaling Model (SDSM) performed an excellent task of reproducing the historical temperature and precipitation patterns in the Khulna Division, although the accuracy was different for each variable. The calibration findings showed that temperature had a higher explained variance (over 70%) than precipitation (around 15%). This is because rainfall in coastal locations is naturally variable and convective. The model's accuracy improved significantly after bias correction, with R^2 values going over 0.82 for maximum and 0.61 for minimum temperatures. Even though precipitation simulation was less dependable, the overall improvement showed that SDSM improves global model outputs for regional-scale studies. Future estimates showed that the temperature will keep rising no matter how much pollution is released. The high-emission RCP8.5 scenario predicts that the minimum temperature would increase by as much as 0.63°C, and the maximum temperature will rise by over 0.99°C by the 2080s. This is consistent with results from other research in Bangladesh and South Asia (Shahid et al., 2021; Haque et al., 2024). The expected increase in temperature means that evapotranspiration will increase, soil moisture will decrease, and salinity stress will increase. These changes might worsen farming and water problems in the area. Precipitation is also expected to rise slowly, from 0.41 mm in the 2020s to 1.28 mm by the 2080s. This means that rainfall will vary more, which aligns with IPCC estimates. The Mann–Kendall trend analysis showed statistically significant positive trends ($p < 0.05$) for temperature and precipitation in all scenarios, especially in RCP8.5 and A2. Spatial analysis indicated that southwestern subdistricts, including Satkhira and Mongla, are anticipated to significantly increase due to their coastline exposure and proximity to the Bay of Bengal. In general, the analysis shows that the Khulna Division will likely see more heat and mild increases in precipitation in the future.

This highlights the need for specific climate adaptation techniques to make agriculture, water, and infrastructure more resilient.

5 Conclusion

Climate change is an inescapable issue in the current world. Global mean temperatures have been increasing rapidly while changes in precipitation have become more erratic and unpredictable. These changes in climatic variables have been affecting various components of the environment and resources such as land, energy, and water resources. This study utilized a widely used downscaling technique, the Statistical Downscaling Model (SDSM), to predict the future climate changes in the Khulna division of Bangladesh. The SDSM was used to translate Global Circulation Models (GCMs) to assess the impact of climate change in the study area under IPCC RCP (used in the fifth assessment report) and SRES (used in the third and fourth assessment reports) scenarios. A quantitative approach was used for model calibration and validation. The model used historical daily data for 1981-2010 as predictand, divided into two data sets of 1980-2000 and 2001-2010 for calibration and validation, respectively. The results were satisfactory for both procedures. After these two steps, the model was used to downscale future climate scenarios. Both models showed an increase in temperature in the 2020s, 2050s, and 2080s under the RCP and SRES scenarios. The results obtained from this study can help policymakers to make decisions and plans for adaptation and mitigation measures for climate change.

6 References

Ahmed, A.U., 2006. Bangladesh climate change impacts and vulnerability: a synthesis. Climate Change Cell, Department of Environment.

Ahmed, N., & Alam, M. M. (2020). Downscaling GCM data for temperature and rainfall projection in coastal Bangladesh. Theoretical and Applied Climatology, 141(1–2), 355–367.

Aizen, E.M., Aizen, V.B., Melack, J.M., Nakamura, T. and Ohta, T., 2001. Precipitation and atmospheric circulation patterns at mid-latitudes of Asia. International Journal of Climatology, 21(5), pp.535-556.

Albani, S., Mahowald, N.M., Perry, A.T., Scanza, R.A., Zender, C.S., Heavens, N.G., Maggi, V., Kok, J.F. and Otto Bliesner, B.L., 2014. Improved dust representation in the Community Atmosphere Model. Journal of Advances in Modeling Earth Systems, 6(3), pp.541-570.

Arora, V.K. and Boer, G.J., 2013. Carbon-concentration and carbon-climate feedbacks in CMIP5 Earth system models. Journal of Climate, 26(15), pp.5289-5314.

Arora, V.K., Boer, G.J., Christian, J.R., Curry, C.L., Denman, K.L., Zahariev, K., Flato, G.M., Scinocca, J.F., Merryfield, W.J. and Lee, W.G., 2009. The effect of terrestrial photosynthesis down regulation on the twentieth-century carbon budget simulated with the CCCma Earth System Model. Journal of Climate, 22(22), pp.6066-6088.

Arora V.K., Friedlingstein, P., Meinshausen, V.K., Jones, C.D., Anav, A., Liddicoat, S.K. and Knutti, R., 2014. Uncertainties in CMIP5 climate projections due to carbon cycle feedbacks. Journal of Climate, 27(2), pp.511-526.

Chen, J., Brissette, F.P. and Leconte, R., 2011. Uncertainty of downscaling method in quantifying the impact of climate change on hydrology. Journal of Hydrology, 401(3-4), pp.190-202.

Chu, J.T., Xia, J., Xu, C.Y. and Singh, V.P., 2010. Statistical downscaling of daily mean temperature, pan evaporation and precipitation for climate change scenarios in Haihe River, China. Theoretical and Applied Climatology, 99(1-2), pp.149-161.

Chylek, P., Li, J., Dubey, M.K., Wang, M. and Lesins, G., 2011. Observed and model simulated 20th century Arctic temperature variability: Canadian earth system model CanESM2. Atmospheric Chemistry and Physics Discussions, 11(8), pp.22893-22907.

Diaz-Nieto, J. and Wilby, R.L., 2005. A comparison of statistical downscaling and climate change factor methods: impacts on low flows in the River Thames, United Kingdom. Climatic Change, 69(2-3), pp.245-268.

Dibike, Y.B. and Coulibaly, P., 2005. Hydrologic impact of climate change in the Saguenay watershed: comparison of downscaling methods and hydrologic models. Journal of Hydrology, 307(1-4), pp.145-163.

Dibike, Y.B. and Coulibaly, P., 2007. Validation of hydrological models for climate scenario simulation: the case of Saguenay watershed in Quebec. Hydrological Processes: An International Journal, 21(23), pp.3123-3135.

Haque, A., Islam, N., Samrat, N. H., & Ray, B. (2021). Smart farming through responsible leadership in Bangladesh. Sustainability, 13(8), 4511.

Huang, C., Barnett, A.G., Wang, X., Vaneckova, P., FitzGerald, G. and Tong, S., (2011). Projecting future heat-related mortality under climate change scenarios: a systematic review. Environmental Health Perspectives, 119(12), pp.1681-1690.

IPCC. (2014). 'Annex II: Glossary', Climate Change 2014: Synthesis Report. Contribution of Working Groups I, II and III to the Fifth Assessment Report of the Intergovernmental Panel on Climate Change, pp.117-130.

IPCC. (2014). Climate Change 2014: impacts, adaptation, and vulnerability. Part B: Regional aspects. Contribution of Working Group II to the Fifth Assessment Report of the Intergovernmental Panel on Climate Change.

IPCC. (2021). Sixth Assessment Report (AR6): Climate Change 2021 – The Physical Science Basis.

Liu, L., Liu, Z., Ren, X., Fischer, T. and Xu, Y., (2011). Hydrological impacts of climate change in the Yellow River Basin for the 21st century using hydrological model and statistical downscaling model. Quaternary International, 244(2), pp.211-220.

Mahmood, M. et al. (2023). Exploring biochar and fishpond sediments to change soil phosphorus. Frontiers in Plant Science, 14, 1224583.

Moriasi, D.N., Arnold, J.G., Van Liew, M.W., Bingner, R.L., Harmel, R.D. and Veith, T.L., (2007). Model evaluation guidelines for systematic quantification of accuracy in watershed simulations. Transactions of the ASABE, 50(3), pp.885-900.

Nasreen, M., Hossain, K. M., & Khan, M. M. (2023). Coastal Disaster Risk Management in Bangladesh. Routledge.

Pohlert, T., Pohlert, M.T., Test, M.K.T., Test, B.U. and Test, S.N.H., (2018). Package trend. Journal of Geophysical Research: Atmospheres, 110(D19).

Rahman, M.I., (2013). Climate change: a theoretical review. Interdisciplinary Description of Complex Systems, 11(1), pp.1-13.

Rahman, M.S., (2013). Climate change, disaster and gender vulnerability: A study on two divisions of Bangladesh. American Journal of Human Ecology, 2(2), pp.72-82.

Salzmann, N., Schaer, C., Rajczak, J. and Kotlarski, S., (2007). Robust climate scenarios for sites with sparse observations: a two-step bias correction approach. International Journal of Climatology, 36(3), pp.1226-1243.

Tuli, R. D., Rashid, K. J., Islam, M. M., Sobhan, M., Islam, S. T., Mondal, K. P., Talukder, B., & Mondal, A. M. (2025). Impact of climatic parameters on spatiotemporal variation of air pollutants across Bangladesh. Urban Climate, 59, 102263. https://doi.org/10.1016/j.uclim.2024.102263

Wells, A.J., Hitchen, J.R. and Parkinson, J.R., (2019). Mushy-layer growth and convection, with application to sea ice. Philosophical Transactions of the Royal Society A, 377(2146), 20180165.

Wetterhall, F., Bárdossy, A., Chen, D., Halldin, S. and Xu, C.Y., (2006). Daily precipitation-downscaling techniques in three Chinese regions. Water Resources Research, 42(11).

Wilby, R.L., Charles, S.P., Zorita, E., Timbal, B., Whetton, P. and Mearns, L.O., (2004). Guidelines for use of climate scenarios developed from statistical downscaling methods. Supporting material of the Intergovernmental Panel on Climate Change.

Wilby, R.L. and Dawson, C.W., (2007). SDSM 4.2-A decision support tool for the assessment of regional climate change impacts user manual. Available at https://sdsm.org.uk/SDSMManual.pdf

Wilby, R.L. and Dawson, C.W., (2013). The statistical downscaling model: insights from one decade of application. International Journal of Climatology, 33(7), pp.1707-1719.

Wilby, R.L., Dawson, C.W. and Barrow, E.M., (2002). SDSM-a decision support tool for the assessment of regional climate change impacts. Environmental Modelling & Software, 17(2), pp.145-157.

World Bank. (2022). Bangladesh Climate and Development Report. Washington, DC.